Academic Journal of Science and Technology
ISSN: 2771-3032 | Vol. 5, No. 3, 2023

Quantitative Characterization of Pore Structure of Carbonate Rocks Based on Micron-CT Technique and Its Seepage Simulation

Mengyuan Cheng[1, a]

[1]College of Resource & Environment, Henan Polytechnic University, Jiaozuo 454003, Henan, China
[a]1060054945@qq.com

Abstract: Micron-CT technology can make up for many shortcomings of traditional rock physics experiments and provide a new platform for rock physics research. In this paper, a 3D digital core model with realistic pore structure characteristics was established using micron-CT scanning combined with advanced image processing techniques with carbonate rocks as the research object. Various morphological algorithms included in the digital core software (Avizo) are applied to quantify and characterize the pore structure of digital cores, and obtain the characteristics of total porosity, effective porosity, pore and throat equivalent radius distribution, and establish an equivalent pore network model. The absolute permeability experiment module was applied in the digital core software (Avizo) to realize the simulation of seepage on the micron scale and calculate the absolute permeability. This paper enriches the existing digital petrophysical research tools by applying digital core software (Avizo), which is of great significance to deepen the understanding of hydrocarbon storage and transport mechanisms inside the reservoir.

Keywords: Carbonate rocks, Micron-CT, Pore structure, Seepage simulation.

1. Introduction

With the development of exploration and development technology and the further increase of the demand for oil and gas resources, the development of unconventional energy has received more extensive attention, among which the dense carbonate reservoirs of unconventional energy have gradually become the focus of oil and gas exploration and development. Compared with conventional oil and gas reservoirs, tight carbonate reservoirs have stronger inhomogeneity. Therefore, it is important to study the microscopic pore structure and seepage characteristics of dense carbonate reservoirs to deeply understand the fluid storage and transport mechanisms inside the reservoirs.

At present, for the study of rock pore structure, domestic and foreign researchers have used different methods to characterize rock pore structure (Chalmers et al., 2012; Clarkson et al., 2012; Curtis et al., 2012; Liu et al., 2015; Liang et al., 2015), and have gained some understanding of the pore structural features have achieved some understanding, such as cast thin sections, scanning electron microscopy (SEM), field emission scanning electron microscopy (FESEM), focused ion beam scanning electron microscopy (FIB-SEM), transmission electron microscopy (TEM), nuclear magnetic resonance (NMR), small angle neutron scattering (SANS), mercury compression (MICP), and low pressure gas adsorption (N2, CO2). However, these studies reflect more two-dimensional information of the pore structure, and it is difficult to obtain information such as three-dimensional distribution of the pore throat, and it is also difficult to describe the pore structure intuitively and accurately and establish the intrinsic connection between such description and fluid percolation properties.

Therefore, many researchers at home and abroad have used micro/nano CT based imaging techniques to study the pore structure characteristics of rocks. Attwood (2006) used the scanned images of X-CT to carry out 3D reconstruction of the pore throat structure of rocks and studied the 3D structural characteristics of the pore throat of rocks; Bera et al. (2011) used micro-CT and FIB-SEM to carry out 3D reconstruction of the Berea sandstone studied the 3D pore structure characteristics of the Berea sandstone; Wang et al. (2009) used micro-CT technology for 3D reconstruction of the pore structure of the core and studied the 3D pore variation pattern of the core; Bai et al. (2013) studied the pore throat distribution and its pore structure characteristics of the dense sandstone of the Yanchang formation using micro/nano multi-scale CT imaging; Tiwari et al. (2013) studied the changes of pore structure during the pyrolysis of oil shale using micro-CT imaging; Golab et al. (2013) studied the 3D reconstruction of pore structure of coal rocks based on micro-CT imaging and studied the 3D pore structure characteristics of coal rocks; Liu et al. (2014) realized the reconstruction of 3D pore structure of sandstone based on micro-CT technology and realized the numerical simulation of various rock physical parameters; Wang et al. (2015) studied the 3D pore structure characteristics of shale based on micro-CT imaging technology to reconstruct the pore structure of Jiulaodong formation shale in 3D. These studies show that domestic and foreign researchers have conducted a large number of studies on the pore structure characteristics of different types of rocks (sandstone, dense sandstone, coal rock, oil shale, shale, etc.) using micro-CT imaging technology and achieved some understanding, which shows that studying the pore structure characteristics of rocks based on micro-CT imaging technology is an effective method and can obtain the 3D distribution of pores and fluid percolation information. However, the results related to the study of 3D pore structure and seepage characteristics of dense carbonate reservoirs in Tahe oil field in Tarim Basin using micro-CT imaging technology need to be studied in depth.

2. Three-dimensional Digital Core Modeling

2.1. Micro-CT imaging

Micro-CT as a new non-destructive testing technique can realize three-dimensional visualization of the internal structure of porous materials, and is currently the most direct and accurate method to establish three-dimensional digital cores. Its principle is the attenuation of X-rays. When X-rays pass through the matrix, inorganic minerals and pore fractures in the core, the attenuation coefficients are different due to the difference in density of these components, so that the purpose of distinguishing pores and rock skeleton can be achieved. In this study, the X-Micro CT (Xradia 510 Versa), introduced by Carl Zeiss AG, was used to acquire three-dimensional images of the cores with a long working distance resolution of up to 1 μm (Fig.1a, b). A series of 993 consecutive 2D slices of 980×1004 voxels with a spatial resolution of 0.6915 μm/voxel were acquired from a cylindrical carbonate rock with a diameter of about 1 mm, and the 3D grayscale images of the sample were obtained by superimposing these 2D slices sequentially. Fig.1c shows the grayscale image of one of the slices with pores and microfractures (dark black) and matrix (gray), which are very easy to identify.

2.2. Image processing

Digital images are usually contaminated by various noises due to factors such as incomplete transmission media, imaging systems and recording devices. These noise signals are not relevant to the study object, appear as useless information and disturb the image observable information, which is not conducive to subsequent quantitative analysis, so the first step of image processing is to enhance the signal-to-noise ratio by filtering algorithms.

Median filter, Gaussian filter, and mean filter are commonly used, but the specific filtering methods need to be considered according to their needs and the final effect of the image. Considering the running time of the computer and the effect of the image after filtering, the median filter of Avizo was chosen to filter the image in 3D. After the median filtering process, the boundary between the pore fracture and matrix becomes more natural, which is beneficial to the subsequent segmentation and extraction of the pore fracture (Fig.1d).

For the extraction of pore models, the most important thing is the threshold segmentation of the image data, which determines the accuracy of the extracted pore models and the reliability of the pore structure. The basic principle of threshold segmentation is to replace an image with multiple levels of gray values by binary pixels and transform it into a binary image containing only two pixel distributions of 0 and 1. The image segmentation threshold (T) can be defined as the grayscale threshold value between the target object (segmented object) and the background object. Let $F(i, j)$ denote the gray value of point (x, y) in the original image, and the gray value of the target object in the segmented image is 1 and the background value is 0. Then, after the binarization process, the gray value $G(i, j)$ of point (x, y) has the following relationship:

$$G(x,y) = \begin{cases} 1, F(i,j) > T \\ 0, F(i,j) < T \end{cases}$$

Considering the difficulty of segmentation and the practical effect after segmentation, the interactive threshold segmentation method in digital core software (Avizo) is used in this thesis. The final segmentation structure is shown in (Fig.1e), and it can be seen that the segmented pore fissures match well with the corresponding image data.

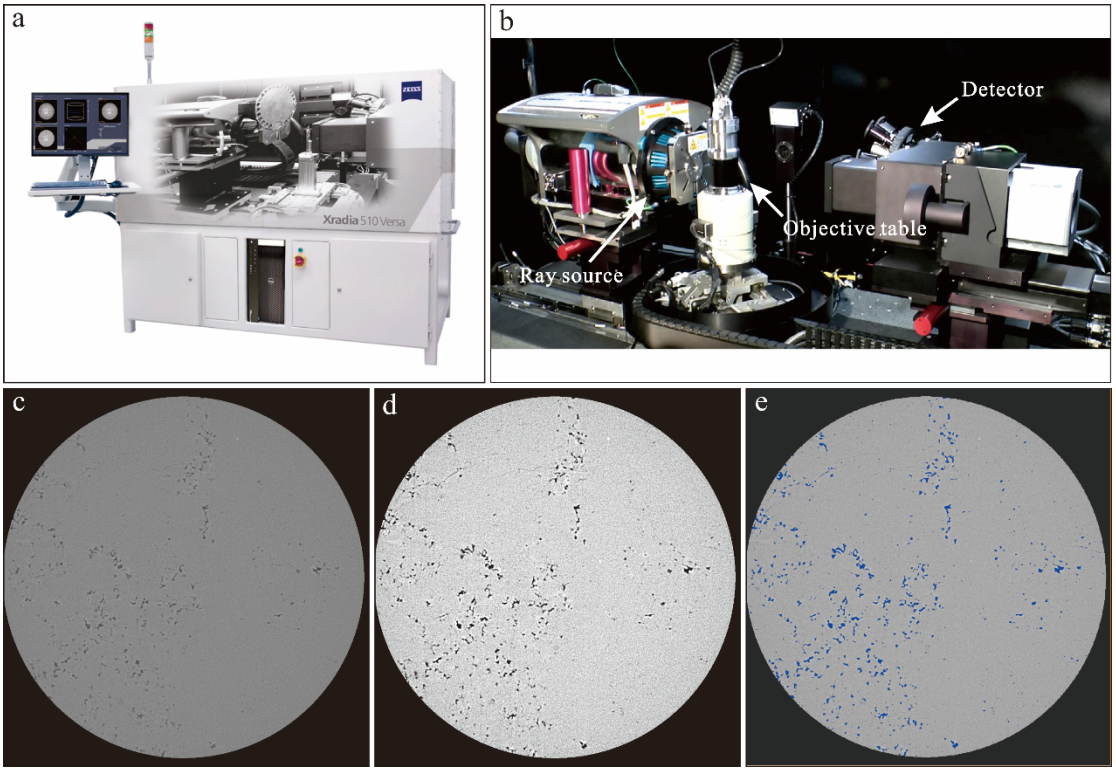

Figure 1. Micron-CT technology flow
(a) micron-CT instrument; (b) internal structure of the instrument; (c) CT section; (d) slice after filtering; (e) binarization result

2.3. Three-dimensional data body construction

Due to the high resolution of this CT 2D slice image, thus causing the original image data to be too large, therefore, the calculation of pore characterization parameters based on the plunger image will not only lead to long data processing time, but also may cause the calculation results to be terminated due to the overload of the computer. Therefore, in order to balance the computation time with the computation results, it is often necessary to extract a subdomain space from the data body to be analyzed that can reflect the overall characteristics for subsequent computation, the representative element volume (REV). The REV is a concept of scale, introduced by Bear (1972) in performing soil seepage analysis, and in digital core analysis, it represents the minimum model size when a computational parameter of the core tends to be stable (Fig.2a). In this study, the porosity φ of the rock was used as a constraint to find the REV, and it was shown through several tests that the porosity value is almost no longer affected by the size when the digital core size is 450 × 450 × 450 voxels (Fig. 2b). Finally, the 3D digital core modeling was completed by rendering in the digital core software (Avizo) using the 3D visualization operation "Volume Rendering" (Fig.3).

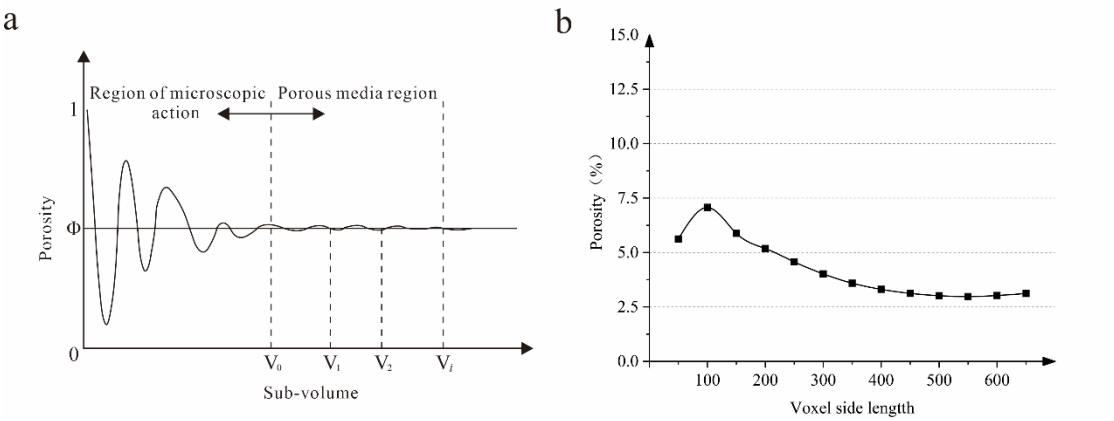

Figure 2. Schematic diagram of REV selection

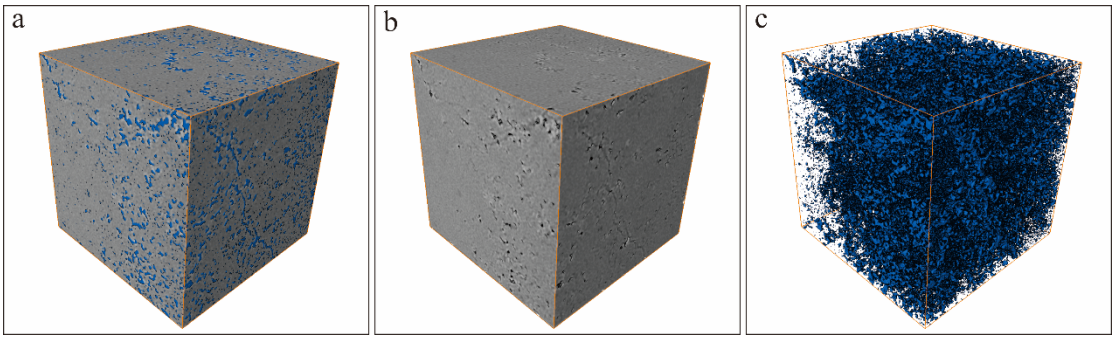

Figure 3. REV digital core model
(a) pores and skeletons; (b) skeleton (transparent pore); (c) pores (transparent skeleton)

3. Digital Rock Physics Experiments

Based on digital cores, a variety of numerical simulation methods and morphological algorithms can be used to quantitatively calculate a wide range of petrophysical parameters, which is the digital petrophysical experiment.

3.1. Quantitative characterization of pore structure

In the pore structure model of the digital core constructed based on the above steps (Fig.3a), most of the pores are in close contact with each other, and it is difficult to distinguish the boundaries of individual pores, which is not conducive to the quantitative characterization of the pore structure at a later stage. For this reason, the boundaries between pores need to be identified and labeled. In this paper, the watershed algorithm is used in the study. The basic principle is to consider the image as a topological landform; the gray value of each pixel in the image represents the elevation of that pixel point, and the higher the gray value, the brighter the area in the image, is compared to a mountain peak; the smaller the gray value, the darker the area in the image, is compared to a catchment basin; the boundary of the catchment basin forms the watershed. The algorithm allows each pore to be clearly identified and labeled uniquely for quantitative analysis (Fig.4a). After determining each pore, the total porosity of the sample can be calculated by the "Arithmetic" algorithm; the effective porosity can also be calculated by the connectivity algorithm "Axis Connectivity" in the digital core software (Avizo) (Tab.1).

Table 1. Statistical table of porosity

total porosity (%)	7.01
effective porosity (%)	2.40

In order to show the topology of the pore space more intuitively, the maximum sphere method is used in this paper, the basic principle of which is to characterize the three-dimensional microscopic pore structure using the maximum

sphere quorum proposed by Silin. based on the basic concept of mathematical morphology (Silin and Patzek, 2006). The basic principle of the maximum sphere method is to find the maximum inner tangent radius of any point in the pore space, and use the local maximum sphere to represent the pore, and the smaller sphere connecting the two local maximum spheres to represent the throat channel, thus forming a "pore-throat-pore" correspondence (Sheng et al., 2019). Thus, an equivalent pore network model that can simplify the characterization of the pore space topology is established (Fig.4b). The yellow sphere in the model represents the equivalent sphere of each segmented pore, and the size of the pore size is displayed according to the equivalent radius, and the larger the equivalent radius of the segmented pore size, the larger the sphere; the blue stick represents the throat channel connecting the pores, and its size is also displayed according to the equivalent radius of the throat channel, and the larger the equivalent radius of the throat channel, the thicker the blue stick. The equivalent radii of the yellow sphere and blue stick are approximately equal to the equivalent radii of the pore and throat at the corresponding locations, and the histogram of the equivalent radii of the pore and throat is finally obtained (Fig.5).

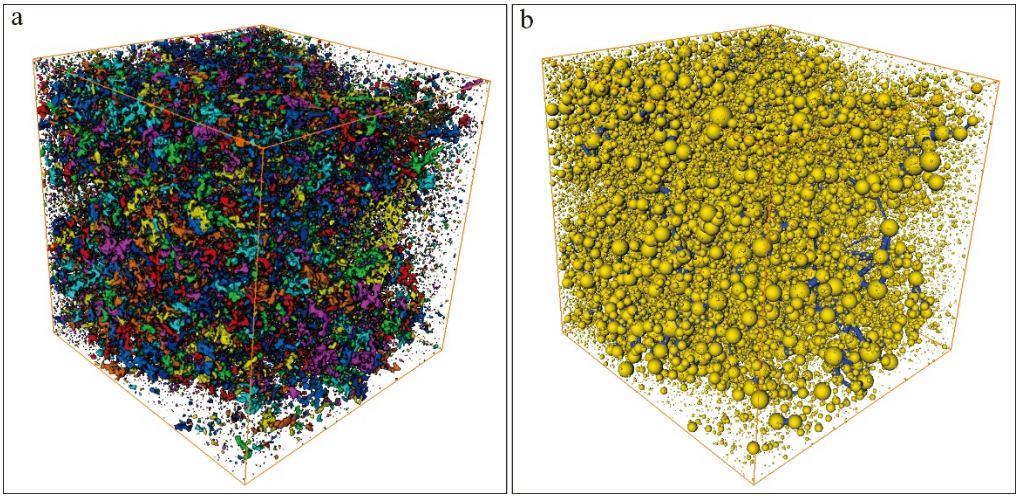

Figure 4. Quantization and characterization of pore structure
(a) pore labeling; (b) pore network model

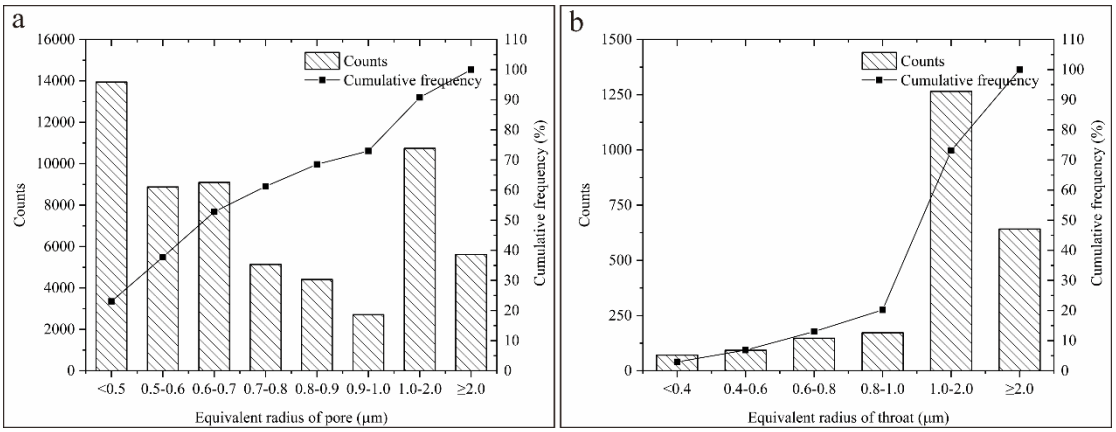

Figure 5. Equivalent radius distribution of pore and throat
(a) pore equivalent radius; (b) equivalent radius of throat

3.2. Numerical simulation of absolute permeability

Absolute permeability is the permeability measured when only one fluid is present in the pores of a rock, when the fluid does not undergo any physical or chemical reaction with the rock, and when the flow of the fluid follows Darcy's law of linear percolation, and is also commonly used as a measure of the ability to transport single-phase fluids in porous materials. Its international system of units is the square meter (m^2), but the square micron (μm^2) is more common because it is almost equal to 1 Darcy (d): 1 d = 0.9869233 μm^2. Absolute permeability is an inherent property of matter and does not depend on any external conditions.

In Darcy's law, the absolute permeability is a constant factor related to fluid, flow and material parameters:

$$\frac{Q}{S} = -\frac{k}{\mu}\frac{\Delta P}{L}$$

where Q is the total flow rate of fluid through the porous medium per unit time, m^3/s; S is the cross-sectional area of fluid through the porous medium, m^2; k is the absolute permeability of the porous medium, m^2; μ is the dynamic viscosity of the flowing fluid, Pa·s; ΔP is the pressure difference applied to the front and rear surfaces of the porous medium, Pa; L is the length of the porous medium in the direction of flow, m. Q/S is often denoted as v, and is used to represent the surface or average velocity of the fluid through the porous medium, the Darcy flow velocity. To numerically

calculate the absolute permeability of the porous medium, the Stokes equation is solved:

$$\begin{cases} \vec{\nabla} \cdot \vec{V} = 0 \\ \mu \nabla^2 \vec{V} - \vec{\nabla} P = \vec{0} \end{cases}$$

where $\vec{\nabla}$ is the Hamiltonian operator; $\vec{V}$ is the velocity of the fluid in the fluid phase of the porous medium; μ is the dynamic viscosity of the fluid; ∇^2 is the Laplace operator; and P is the pressure of the fluid in the fluid phase of the porous medium.

This system of equations is a simplification of the Navier-Stokes equations, taking into account: (i) an incompressible fluid, which means that its density is constant; (ii) a Newtonian fluid, which means that its dynamic viscosity is a constant; (iii) a steady-state flow, which means that the velocity does not vary with time; and (iv) a creeping flow, which means that the velocity in question is sufficiently small not to produce turbulence. Once this system of equations is solved, Darcy's law can be applied to calculate the absolute permeability. All values of this equation can be derived from the solution of the system of equations ($Q, \Delta P$) or the external conditions (S, L, μ).

The boundary conditions used in the numerical simulation method are: (i) no slip occurs at the fluid-solid interface; (ii) a solid plane of voxel width not perpendicular to the flow direction is added to the image surface to isolate the pore space from the outside world and ensure that no fluid flows out of the system; and (iii) an experimental device is added to the boundary perpendicular to the flow direction. Considering the stratigraphic pressure and physical properties of the fluid at the study level, the absolute permeability experimental module in the digital core software (Avizo) was used in this paper, whose default inlet pressure is 0.13 MPa, outlet pressure is 0.1 MPa, and flow viscosity is 0.001 Pa-s. The final velocity field flow diagrams in the horizontal (X, Y) and vertical (Z) directions (Fig.6) and the corresponding absolute permeability values (Tab.2).

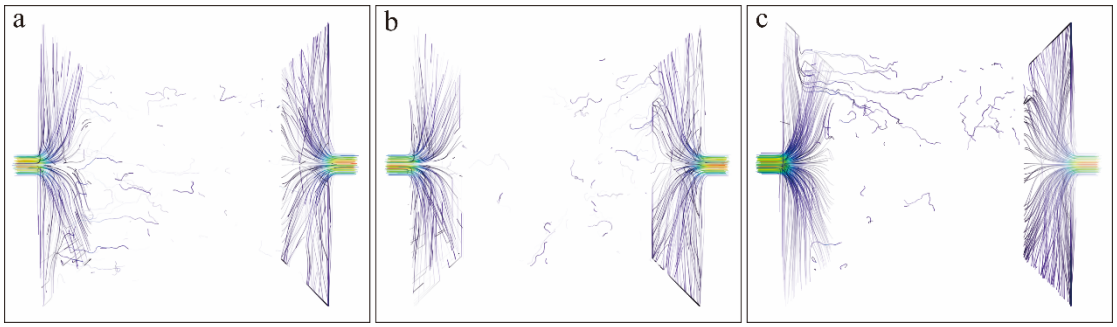

Figure 6. Velocity field streamlines in horizontal (X, Y) and vertical (Z) directions
(a) horizontal X-direction; (b) horizontal Y-direction; (c) vertical Z-direction

Table 2. Permeability statistics

Permeability (mD)	X-direction	4.51
	Y-direction	5.74
	Z-direction	5.14

4. Conclusion and Prospect

(1) Digital cores built by using micro-CT scanning combined with digital core software (Avizo) can finely capture the real pore structure characteristics of rocks, and digital petrophysical experiments based on digital core models can accurately obtain the total porosity, effective porosity, pore and throat equivalent radius distribution characteristics, and pore network models that can simplify the characterization of pore space topology; (2) The absolute permeability experiment module in digital core software (Avizo) is used to visually simulate the fluid percolation process in real pore space and calculate the absolute permeability. The absolute permeability experiment module in the digital core software (Avizo) can visually simulate the fluid percolation process in the real pore space, and calculate the absolute permeability. With the development of computer technology, digital petrophysics will definitely become an important technical tool to participate in the development and construction of oil and gas fields.

References

[1] Attwood D. 2006. Microscopy: Nanotomography comes of age [J]. Nature, 442(7103): 642-643.

[2] Bai B, Zhu R K, Wu S T, Yang W J, Jeff G, Allen G, Zhang X X, Su L. 2013. Multi-scale method of Nano (Micro)-CT study on microscopic pore structure of tight sandstone of Yanchang Formation, Ordos Basin [J]. Petroleum Exploration and Development, 40(3): 329-333.

[3] Bear J. 1972. Dynamics of fluids in porous media. Elsevier, New York.

[4] Bera B, Mitra S K, Vick D. 2011. Understanding the micro structure of Berea Sandstone by the simultaneous use of micro-computed tomography (micro-CT) and focused ion beam-scanning electron microscopy (FIB-SEM) [J]. Micron, 42(5): 412-418.

[5] Chalmers G R, Bustin R M, Power I M. 2012. Characterization of gas shale pore systems by porosimetry, pycnometry, surface area, and field emission scanning electron microscopy/transmission electron microscopy image analyses: Examples from the Barnett, Woodford, Haynesville, Marcellus, and Doig units [J]. AAPG Bull, 96(6): 1099-1119.

[6] Clarkson C R, Freeman M, He L, Agamalian M, Melnichenko Y B, Mastalerz M, Bustin R M, Radliński A P, Blach T P. 2012a. Characterization of tight gas reservoir pore structure using USANS/SANS and gas adsorption analysis [J]. Fuel, 95, 371-385.

[7] Curtis M E, Sondergeld C H, Ambrose R J, Rai C S. 2012. Microstructural investigation of gas shales in two and three dimensions using nanometer-scale resolution imaging [J]. AAPG Bull, 96(4): 665-677.

[8] Golab A, Ward C R, Permana A, Lennox P, Botha P. 2013. High-resolution three-dimensional imaging of coal using microfocus X-ray computed tomography, with special

reference to modes of mineral occurrence[J]. International Journal of Coal Geology, 113: 97-108.

[9] Liang L X, Xiong J, Liu X J. 2015. Mineralogical， microstructural and physiochemical characteristics of organic-rich shales in the Sichuan Basin, China [J]. Journal of Natural Gas Science and Engineering, 26: 1200-1212.

[10] Liu X J, Xiong J, Liang L X. 2015. Investigation of pore structure and fractal characteristics of organic-rich Yanchang formation shale in central China by nitrogen adsorption / desorption analysis [J]. Journal of Natural Gas Science and Engineering, 22: 62-72.

[11] Liu X J, Zhu H L, Liang L X. 2014. Digital rock physics of sandstone based on micro CT technology[J]. Chinese Journal of Geophysics, 57(4): 1133-1140.

[12] Sheng J, Yang X J, Li G, Xu L, Li Y N, Wang J R, Zhang C Y, Cui H D. 2019. Application of Multiscale X-CT Imaging Digital Core Technique on Observing Micro-pore Structure of Carbonate Reservoirs[J]. Geoscience, 33(3): 653-661.

[13] Silin D, Patzek T. 2006. Pore space morphology analysis using maximal inscribed spheres[J]. Physica A: Statistical Mechanics and its Applications, 371(2): 336-360.

[14] Tiwari P, Deo M, Lin C L, Miller J D. 2013. Characterization of oil shale pore structure before and after pyrolysis by using X-ray micro CT[J]. Fuel, 107: 547-554.

[15] Wang J L, Gao J, Liu L. 2009. Porosity characteristics of sandstone by X-ray CT scanning system [J]. ACTA PETROLEI SINICA, 30(6): 887-893.

[16] Wang Y, Pu J, Wang L H, Wang J Q, Jiang Z, Song Y F, Wang C C, Wang Y F, Jin C. 2015. Characterization of typical 3D pore networks of Jiulaodong formation shale using nano-transmission X-ray microscopy[J]. Fuel, 170: 84-91.